IVYSPRING INTERNATIONAL PUBLISHER

Theranostics

2015; 5(8): 787-795. doi: 10.7150/thno.11139

Research Paper

A Prodrug-type, MMP-2-targeting Nanoprobe for Tumor Detection and Imaging

Yaping Wang[1,2], Tingting Lin[1,2], Wenyuan Zhang[2], Yifan Jiang[2], Hongyue Jin[2], Huining He[1], Victor C. Yang[1,3], Yi Chen[2], Yongzhuo Huang[2]✉

1. Tianjin Key Laboratory on Technologies Enabling Development of Clinical Therapeutics and Diagnostics, School of Pharmacy, Tianjin Medical University, Tianjin 300070, China.
2. Shanghai Institute of Materia Medica, Chinese Academy of Sciences, 501 Hai-ke Rd, Shanghai 201203, China.
3. University of Michigan, College of Pharmacy, 428 Church St, Ann Arbor, MI 48108, USA.

✉ Corresponding author: Tel: +86-21-2023-1000 ext 1401; E-mail: yzhuang@simm.ac.cn

Received: 2014.11.22; Accepted: 2015.02.18; Published: 2015.04.06

Abstract

Tumor-associated proteases (TAPs) have been intensively studied because of their critical roles in cancer development. As a case in point, expression of matrix metalloproteases (MMP) is significantly up-regulated in tumorigenesis, invasion, and metastasis among a majority of cancers. Here we present a prodrug-type, MMP-2-responsive nanoprobe system with high efficiency and low toxicity for detecting MMP-2-overexpressed tumors. The nanoprobe system is featured by its self-assembled fabrication and FRET effect. This prodrug-type nanoprobe is selectively activated by MMP-2, and thus useful for detection of the MMP-2-overexpressed cells and tumors. The nanoprobe system works successfully in various animal tumor models, including human fibrosarcoma and subcutaneous glioma xenograft. Furthermore, in order to overcome the blood brain barrier (BBB) and achieve brain tumor targeting, a transferrin-receptor targeting peptide (T7 peptide) is strategically incorporated into the nanoprobe. The T7-functionalized nanoprobe is capable of detecting the orthotopic brain tumor, with clear, real-time in vivo imaging. This method is promising for in vivo detection of brain tumor, and real-time monitor of a TAP (i.e., MMP-2).

Key words: matrix metalloprotease; protease-activatable probe; tumor imaging; brain tumor; fluorescence resonance energy transfer.

Introduction

Malignant tumors as the major global public health problem impose great threats to humans. Early detection is the most important factor for completely curing cancer. The overexpression of tumor-associated proteases (TAPs) is the prominent feature in carcinogenesis, and TAPs play a pivotal role in cancer progression via the regulatory mechanism of proteolysis.[1] Among them, matrix metalloproteases (MMPs) comprise a family of zinc-dependent secreted endopeptidases crucial for regulating degradation and procession of extracellular matrixes.[2, 3] MMPs are involved in tumor-associated angiogeneisis, tumor growth, progression, and metastasis, with overexpression in many human solid tumors, thus serving as a biomaker.[4]

Among the currently known MMPs, MMP-2 is frequently overexpressed in the majority of solid tumors such as breast, colon and prostate cancers, and its significant role in promoting cancer progression [5] renders it an important target for tumor diagnosis and therapy. [6-8] Therefore, development of sensitive detection of MMP-2 offers a great value for tumor monitoring.

Fluorescence resonance energy transfer (FRET)-based strategy has been generally used for design of protease-activatable probes, featured by a

hairpin-like peptide backbone (containing a protease substrate sequence) with a FRET paired dyes at each end. [9] Synthesis of the hairpin-structured peptide is difficult and pricy, because the D-form sequences must be used for reducing non-specific cleavage in the blood. We previously developed a FRET-based quantum-dot system for detecting the cysteine protease legumain. [10] Here, we further developed a self-assembling FRET-based nanoprobe that is responsive to MMP-2. Such system is comprised of two units: (1) the fluorophore unit—low-molecular-weight heparin (LMWH) modified quantum dots (LMWH-QD); and (2) the quencher unit—activatable low-molecular-weight protamine (ALMWP) modified QSY21 dye (QSY-ALMWP) (**Scheme 1**). This nanoprobe was characterized by its self-assembling between the fluorophore and quencher units. Self-assembly was processed via the strong and stable affinity between anionic heparin and cationic protamine. Unlike the conventional chemical conjugation, the noncovalent linkage of LMWH/LMWP offers a simple method for binding the fluorophore and quencher units together for achieving FRET effect. The ALMWP contains an MMP-2 substrate sequence that serves as a cleavable spacer between QSY21 and LMWP. Once inside the tumor, the QSY21 would detach from the nanoprobe, in response to the catalysis mediated by MMP-2.

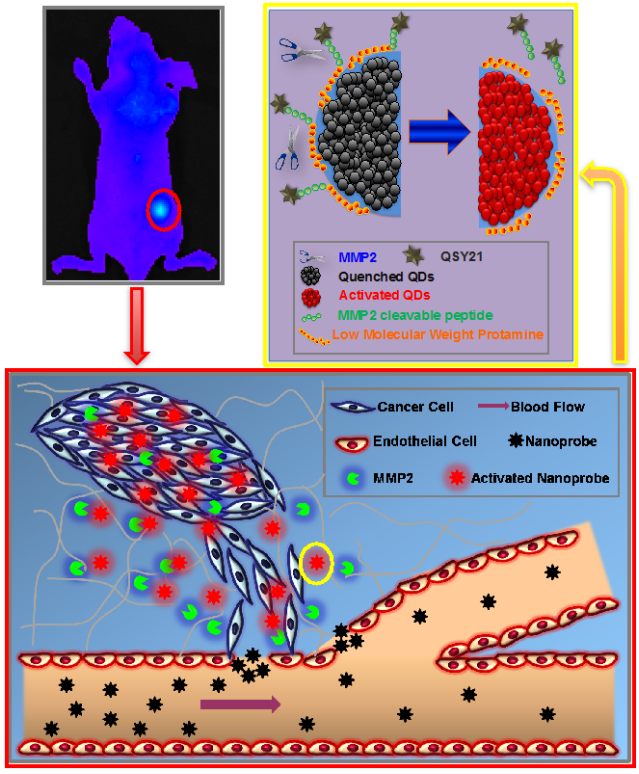

Scheme 1. The MMP-2-activatable nanoprobe. By intravenous administration, the nanoprobe will accumulate at the tumor due to the EPR effect. The MMP-2 cleavable peptide linker will be cleaved preferentially by MMP-2 overexpressed in the tumor. With detachment of the QSY21 quencher, the fluorescence of QD will recover.

LMWH was used for surface modification. Apart from functioning as linkage with LMWP, LMWH could also improve biocompatibility of the QDs and reduce nonspecific uptake of QDs by reticuloendothelial system. The nanoprobes would benefit from the enhanced permeation and retention (EPR) effect for tumor accumulation.

It should be pointed out that LMWP (sequence: VSRRRRRRGGRRRR), identified from the enzymatic digestion of protamine, has been applied as a cell-penetrating peptide for intracellular delivery of biomacromolecules and nanoparticles.[11-13] Therefore, after cleavage, the exposure of LMWP may be beneficial for increasing cellular uptake of the activated probe.

In this study, we investigated the in vivo imaging application of the nanoprobe with multiple animal tumor models with MMP-2 expression.

Experimental section

Synthesize of the prodrug-type nanoprobe

(1) *Preparation of 3-mercaptopropionic acid (MPA)-coated CdTe quantum dots (QD-MPA)* QD-MPA was prepared using aqueous-phase synthesis. In brief, NaHTe was prepared by incubation of the solution containing Tellurium powder (0.2 mmol) and $NaBH_4$ (1.3 mmol) at 80 ^oC for 1 h under the protection of N_2. The mixture of $CdCl_2$ solution (0.2 mmol) and MPA solution (0.34 mmol) with pH of 12 was added to the NaHTe solution (0.02 mmol) with reaction ratio of 1:1.7:0.1 (Cd: MPA: Te), and heated to reflux under N_2 flow. The thus-formed QD-MPA was purified using isopropanol-precipitating method, followed by vacuum dry.

(2) *Preparation of QD-LMWH* QD-LMWH was prepared by a ligand-exchange method. First, LMWH (50 mg) was oxidized by sodium periodate in 10 mL citric acid buffer (0.1 M, pH 7.0) at a molar ratio of 1:1.5 (sodium periodate : LMWH repeating unit). The periodate-oxidized LMWH was reacted with cysteamine hydrochloride (11 mg) in 20 mL phosphate buffer (0.1 M, pH 7.0). Thiolated LMWH (LMWH-SH) was obtained by reduction using sodium borohydride and purification by dialysis. Second, the LMWH-SH was added to the QD-MPA solution (OD_{310nm} = 1.0) in PBS (pH 7.4) for overnight incubation at room temperature. The resultant QD-LMWH was purified using the isopropanol-precipitating method and vacuum dry.

(3) *Preparation of QSY–ALMWP* The activatable LMWP (ALMWP) containing LMWP-MMP-2 cleavable substrate (PLGVR) was synthesized via a standard solid phase method (sequence: KGGPLGVRGGVSRRRRRRGGRRRR, with acetylated

N-terminus and amidated C-terminal). ALMWP in DMSO (10 μg/mL), via the ε-amino group on the terminal lysine, was reacted with QSY21-NHS ester (1.3 : 1 mol/mol) in the presence of 1% N-Methylmorpholine for 48 h. The product, termed as QSY–ALMWP, was determined and purified using the reversed-phase C_{18} high-performance liquid chromatography (HPLC).

(4) *Self-assembly of QSY–ALMWP with LMWH–QD* The self-assembling nanoparticles was prepared by mixing QSY–ALMWP, in a range of 0–32 μg, with LMWH–QD (32 μg) in deionized water. The mixtures were incubated for 30 min at room temperature. The FRET efficiency of the prepared nanoprobe (QSY-QD) was monitored by measuring the fluorescence intensity using a fluorospectrometer (Hitachi, F4600, Japan).

Characterization of the activatable nanoprobe

Size analysis and ξ potential of the activatable nanoprobe were performed using Zetasizer Nano-ZS90 (Malvern, UK). The morphology was observed using transmission electron microscopy (TEM) operating at an accelerating voltage of 100 kV (JEOL JEM-1200EX, Japan). Fluorescence intensity was measured using a fluorospectrometer.

Cell lines

Human embryonic kidney 293T cells, human umbilical vein endothelial cells (HUVEC), human fibrosarcoma HT1080 cells, human breast cancer MCF7 cells, mouse melanoma B16 cells, human cervical cancer HeLa cells, and human colon cancer SW620, human glioma U87 cells were incubated in cell culture medium containing 10% FBS and 1% antibiotics at 37 ^{o}C in humidified atmosphere and 5% CO_2.

Cellular activation of the MMP-2-responsive nanoprobe

Cell-specific activation of the nanoprobe was performed in various cell lines. The nanoprobe was incubated with cells for 4 h. Cells were then washed with PBS for three times and fixed with 4% paraformaldehyde. Extracellular fluorescence was quenched using trypan blue. Cells were observed using a fluorescence microscope (Olympus, Japan). Furthermore, the cellular activation efficiency was quantitatively measured by fluorescence-activated cell sorting (FACS) (BD, USA). In brief, the cells were exposed to the medium containing the nanoprobe for 4 h. After thorough wash with PBS, the cells were collected and subjected to FACS analysis.

Western blotting analysis of MMP-2 in various cell lines

(1) *Preparation of cell extracts* The cells were lysed for 30 min on ice with 100 μL/well of cell lysis buffer containing 1% protease inhibitors (Beyotime, China) under constant shaking, and scraped with a rubber policeman. The cell lysates were centrifuged at 14,000 r/min for 15 min, and the supernatants collected for MMP-2 western blotting assay.

(2) *Preparation of cell medium* Cells grew to 80% confluency in 24-well plates. After washing twice with PBS, serum-free medium were added to cell wells and incubated for 24 h, and then the cell medium was collected and centrifuged at 14,000 r/min for 15 min. The supernatants were used for MMP-2 western blotting assay.

(3) *Western blotting assay* The total protein concentrations in cell extract and cell medium were determined by a standard BCA method. Sample proteins were resolved using 5% (w/v) stacking and 10% (w/v) resolving PAGE gels. Antibodies of MMP-2 (1:500; Abcam) and β-actin (1:20000; Beyotime) were used as the first antibodies. Horseradish peroxidase-conjugated anti-rabbit IgG, and anti-mouse IgG (Santa Cruz Biotechnology) were used as the second antibodies according to the manufacture's protocol. Detection was performed by using the gel imaging analysis system.

Xenograft tumor animal models

Balb/c nude mice (4–5weeks old, 18–22g) were housed under specific pathogen-free conditions with a 12 h light/dark cycle. Animals possessed continuous access to sterilized food pellets and distilled water. All animals were in quarantine for a week before treatment. The experimental procedures were approved by the Institutional Animal Care and Use Committee.

The HT1080 xenograft tumor model or MCF-7 model was established by inoculating 1×10^6 cells subcutaneously into the back of nude mice.

Ex vivo activation study

The mice bearing HT1080 tumor were killed and the major organs (heart, liver, spleen, lung, kidney, and tumor) collected for cryosection. The tissue slides were divided into two experimental groups: the enzyme-inactivated group that was exposed to 4% glutaraldehyde to denature MMP-2, and the enzyme-active group. The slides were treated with the activatable QD for 30 min at room temperature, stained with DAPI, and mounted with glycerin jelly. The fluorescence was observed with a fluorescence microscope (Olympus, Japan).

The mice bearing with HT1080 tumor were *i.v.* injected with nanoprobe for 24 h. FITC-lectin was injected for labelling tumor blood vessels, and then the animals were killed and the tumor was collected for cryosection. The fluorescence was observed with a fluorescence microscope (Olympus, Japan).

In vivo tumor imaging

The mice bearing HT1080 tumor were given the prodrug-type nanoprobes (200 μl, 0.5 mg/ml) via tail intravenous injection for imaging studies. Fluorescence activated by MMP-2 was captured using the IVIS imaging system (Caliper Life Science), and analyzed using Living Image (Caliper Life Sciences). The signal intensity was quantified as the flux of all detected photon counts by repeating triple measurement within a constant area of the region of interest (ROI).

Furthermore, the xenografted glioma animal model was established by subcutaneously inoculating 1×10^7 U87 cells into the back of the BALB/c nude mice. The mice bearing the U87 tumor were subjected to in vivo imaging studies. The nanoprobes were injected via tail vein for tumor imaging with the IVIS imaging system.

Orthotopic glioma animal model was also developed by inoculating the U87-Luc cells (stably expressing firefly luciferase) into the left cerebral hemisphere using a stereotaxic apparatus. The bioluminescence imaging was performed to monitor the orthotopic tumor growth by giving the substrate luciferin into the abdominal cavity of the mice at a dose of 150 mg/kg body weight. In order for improving brain delivery, a brain-targeting sequence (HAIYPRH, termed T7) [14] was added to the original ALMWP, thus forming a T7-ALMWP hybrid peptide (HAIYPRH $_{(QSY21)}$KGGPLGVRGGVSRRRRRRGGRRRR). The T7-ALMWP, taking the place of ALMWP, was used to prepare the nanoprobe for the orthotopic glioma imaging. In brief, the self-assembly of $T7_{(QSY)}$-ALMWP with LMWH-QD nanoparticles was prepared by mixing $T7_{(QSY)}$-ALMWP with LMWH-QD in deionized water. The mixtures were incubated for 30 min at room temperature. The FRET efficiency of the thus-formed nanoprobe was monitored by measuring the fluorescence intensity. It was carried out by injection of the nanoprobe via tail vein, and in vivo fluorescent images were captured at various time points.

In vitro and *in vivo* biosafety study of the nanoprobe

The cytotoxicity was studied in non-tumoral cell lines of 293T and human umbilical vein endothelial cell (HUVEC). The cell viability was measured by a standard MTT assay.

Fifteen KM mice (18–22 g) were used and divided into three groups—the blank, QD-LMWH, and nanoprobe groups—for preliminary safety evaluation. The body weight changes, organ coefficient were recorded, and major organs were processed by histological examination.

Statistical analysis

The quantitative data were expressed as mean ± SD. Statistical analysis was performed by Student's t-test. Results were considered statistically significant if the P value less than 0.05.

Results and discussions

Characterization of the nanoprobe

Heparin is a natural polysaccharide with biocompatible, biodegradable, and water-soluble properties. Recent studies have shown that heparin has a variety of anticancer activities including inhibition of angiogenesis, suppression of metastasis and tumor growth. [15, 16] In our study, LMWH was used as a unit for non-covalently binding with LMWP. Moreover, the LMWH modification greatly improved colloidal stability of the QDs, and significantly reduced the toxicity of the QDs.

ALMWP (sequence: KGGPLGVRGGVSRRRR RRGGRRRR) contains MMP-2 substrate linker sequence (PLGVR) and LMWP (VSRRRRRRGGRRRR). Bi-glycine (GG) was used as a flexible peptide tether for improving the access of MMP-2 to the substrate sequence. The characterization of the QSY-ALMWP is shown in **Figure S1** (Supplementary Materials).

The emission wavelength of the QD developed in this study ranges from 640 nm to 680 nm, and characterization results are shown in Supplementary Material: **Figure S2**. The dark quencher QSY21 has a broad and intense absorption (540–750 nm) but no fluorescence making it useful as an efficient acceptor of the far red and near-infrared fluorescent probes in FRET applications. [17]

The nanoprobe was synthesized through a self-assemble method based on the electrostatic affinity between LMWH and LMWP. The fluorescence intensity was determined with the varying w/w ratio (QSY-ALMWP/LMWH-QD) for evaluating the FRET effect. Fluorescence intensity was decreased along with the elevating ratio, and reached a platform at the w/w ratio of 2.5:1 (Supplementary Material: **Figure S3**), indicating the binding site saturation. Therefore, the ratio of QSY-ALMWP/LMWH-QD was set at 2.5:1 for the subsequent studies. Because protamine can substitute LMWP to bind with heparin, the QD was detached from its quencher by adding protamine, and the highly efficient fluorescence recovery was ob-

served (**Figure 1A**), demonstrating the activatable feature of the FRET-based nanoprobe. Of note, the binding affinity between LMWH and LMWP is very stable, and serum proteins cannot compete for the binding (Supplementary Material: **Figure S4**).

The particle size of prodrug-type nanoprobe was 204 nm with PDI of 0.150 (**Figure 1B-C**), and would benefit from the EPR effect for tumor accumulation. The negative ζ potential (**Figure 1D**) would favorably reduce nonspecific binding with serum proteins in blood.

Cellular and *ex vivo* activation

MMP-2-induced activation of the prodrug-type nanoprobe was investigated in several cell lines (**Figure 2**). The results showed that the nanoprobe was highly activated in HT1080 cells with MMP-2 overexpression. Only minor activation was found in other tumor cells, such as MCF-7, B16, HeLa, and SW620 cells. Of note, during the endocytosis process, fluorescence in lysosomes was hardly observed in the 293 cells without MMP-2 expression, suggesting that the non-specific activation in lysosomes imposed insignificant effect on imaging. It also could be accounted for the low cellular uptake of the inactivated nanoprobe. However, once cleavage by MMP-2, the exposed LMWP could mediate cell entry, because LMWP can function as cell-penetrating peptide.

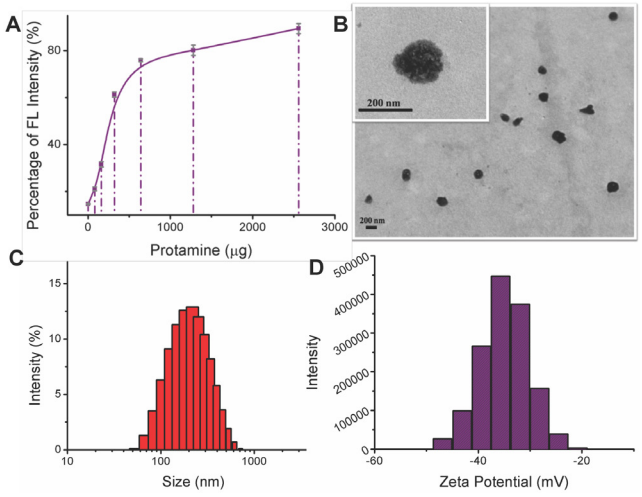

Figure 1. (A) Fluorescence recovery of the nanoprobe with addition of protamine. The more the ALMWP-QSY added, the less the fluorescence intensity will be. (B) TEM images of the prodrug-type nanoprobe. Size distribution (C) and ζ potential (D) of the nanoprobe.

The quantitative activation efficiency of the nanoprobe was measured by using FACS. It was well in accordance with the cell imaging observation that the highest median fluorescence value of 133 was determined in HT1080 cells, compared to that of 31 in MCF7 cells, 16 in B16 cells, 22 in Hela cells and 24 in SW620 cells. Lowest level (i.e. 6.4) was found in the non-tumoral 293T cell line.

There are two forms of presence of MMP-2 (i.e., secreted and membrane-bound forms), including the pro-matured (72 kDa) and matured (66 kDa) status of MMP-2. Both statuses were found in the membrane-bound MMP-2 in the HT1080 cells (**Figure 2D**). By contrast, there was mainly the matured status in the secreted MMP-2 (**Figure 2E**). However, it should be mentioned that both statuses were found to possess enzymatic activity according to the gelatin zymography results,[18] because there are multiple mechanisms involved in MMP-2 activation, e.g., phosphorylation and cysteine switch,[18, 19] but not limiting to propeptide cleavage.

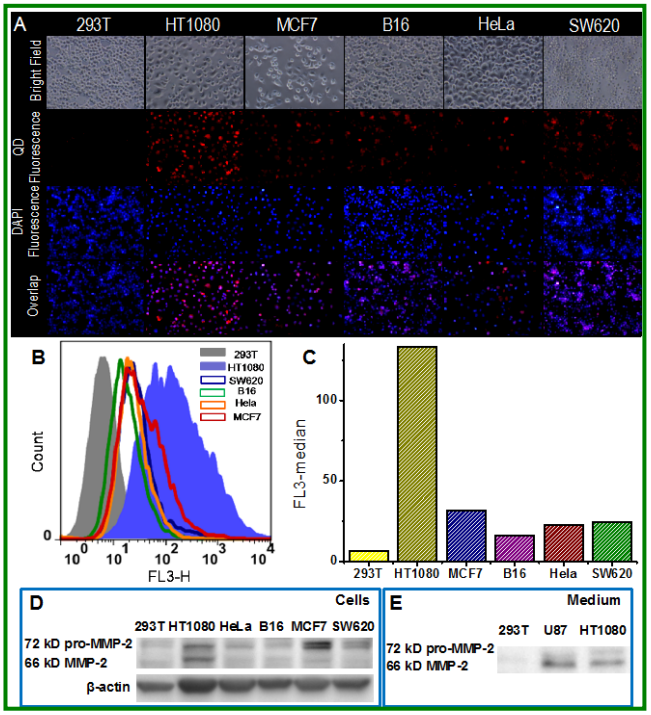

Figure 2. (A) Varying degrees of MMP-2-induced activation in 293T cells, HT1080 cells, MCF7 cells, B16 cells, Hela cells and SW620 cells. Images were presented as bright field, QD fluorescence (red), DAPI fluorescence (blue) and overlap images. (B) FACS assay for MMP-2-induced activation of the nanoprobe in 293T cells, HT1080 cells, MCF7 cells, B16 cells, Hela cells and SW620 cells. (C) The median fluorescence intensity observed in 293T cells, HT1080 cells, MCF7 cells, B16 cells, Hela cells and SW620 cells. Western blotting analysis of MMP-2 in cell lysis (D) and medium (E).

To study the MMP-2-specific activation effect of the prodrug-type nanoprobe, tumor and other major organs were collected from the mice bearing xenografted HT1080 tumor, and the cryosection of each tissue was processed. The nanoprobes were efficiently activated in the tumor slices, showing red fluorescence (**Figure 3**). By contrast, in the enzyme-deactivated tumor slides, which were pretreated with glutaraldehyde, the nanoprobe could not activated and remained quenched. Moreover, the nanoprobe was also applied to the slices of other or-

gans (e.g. heart, liver, spleen, lung, and kidney), and very minor fluorescence was found in those slices. The results demonstrated that the nanoprobe was preferentially activated by the tumor with overexpression of the MMP-2, indicating the in vivo selectivity for tumor imaging.

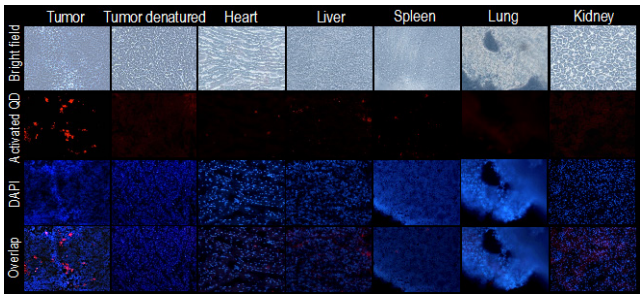

Figure 3. Ex vivo detection of the tumor-activatable nanoprobe. Images were presented as bright field, QD fluorescence (red), DAPI fluorescence (blue), and overlap images.

In vivo activation

To explore the feasibility of in vivo tumor imaging, after tail vein injection of the nanoprobe, the animals were subjected to the IVIS imaging system. In vivo imaging was conducted at 1, 2, 6 and 7 h. The increased fluorescence intensity in tumor clearly distinguished it from other tissues (**Figure 4A&B**). The activation was quick (within 0.5 h) and preferential in tumor, indicating the sensitivity and specificity for tumor detection and imaging.

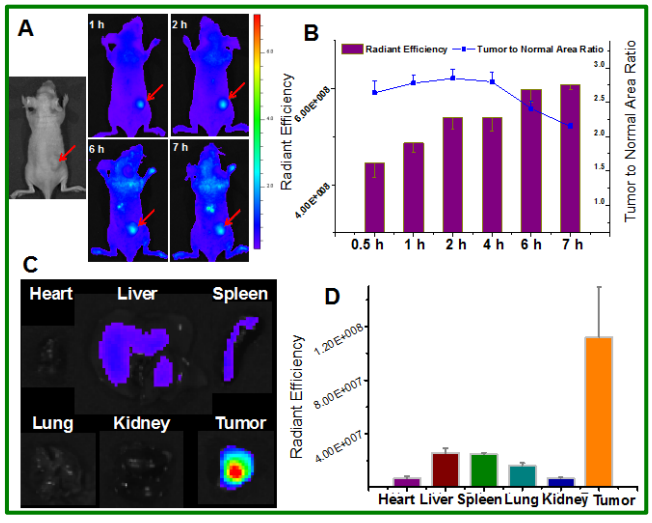

Figure 4. In vivo imaging for HT1080 tumor model with overexpression of MMP-2. (A) Fluorescence images taken before injection and various time points after i.v. injection. (B) The radiant efficiency and tumor to normal area ratio in the tumor site. (C) Ex vivo tissue imaging at the experimental endpoint. (D) Radiant efficiency in the collected tissues.

The major organs were collected 24 h after *i.v.* injection for ex vivo imaging. A clear tissue distribution was observed in **Figure 4C&D**. The nanoparticles tend to accumulate in the organs with rich blood supply, such as the liver, which is of highly metabolic activity, and active degradation thereby would cause undesired fluorescence recovery. However, the fluorescence intensities in tumor were 16.4, 4.3, 4.5, 6.9, and 15.7 times higher than that in the heart, liver, spleen, lung, and kidney, respectively. The results verified that the prodrug-type nanoprobes could be efficiently activated and accumulated in tumor compared to other tissues, achieving effective and preferential tumor imaging through *i.v.* administration.

We further studied in vivo activation by giving the nanoprobe to mice bearing tumor xenograft via tail vein injection. The tumor tissues were collected for cryosection process, and the slices were observed using fluorescence microscopy. The intense fluorescence was found in the HT1080 tumor with MMP-2 overexpression, indicating the efficient tumor accumulation and activation. The activated nanoprobes mainly distributed close to the blood vessels (green staining) tumor, suggesting the leakage of the tumor vessels, through which the nanoprobe penetrated into the interstitial space via EPR effect. Very minor activation, however, was observed in the xenografted SW620 tumor, in accordance with its low MMP-2 expression.

It should be mentioned that although the MMP-2 expression was found similar in the cultured cells of HT1080 and MCF-7, there was significant difference observed in vivo—high expression in HT1080 tumor xenograft but only moderate level in the MCF-7 xenograft (**Figure 5C**). The expression of tumor-associated proteases could be regulated by the tumor microenvironment.

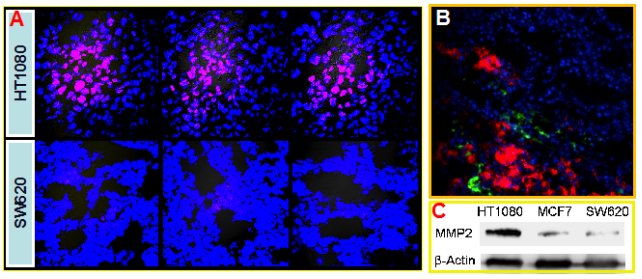

Figure 5. (A) Tumor-associated activation of the nanoprobe. (B) Blood vessel staining (green) and the activated nanoprobe (red) in HT1080 tumor. (C) Western blotting analysis of MMP-2 in HT1080, MCF-7, and SW620 tumor.

The nanoprobe was also tested for tumor-associated activation in MCF-7 xenografted tumors. The MCF-7 tumor still could be identified at 1-2 hour post-injection; the activation efficiency was relatively weak yet clearly distinguishable. The fluorescence signal in tumor displayed more than 2-fold higher than that of the adjacent tissue area (**Figure**

6A&B).

Moreover, in order to evaluate the non-specific activation effect in vivo, the nanoprobe was given via intramuscular injection (right thigh) to the mice. Little fluorescence was activated and detected in the injection site within 2.5 h (**Figure 6C&D**). The results demonstrated that the nanoprobe cannot be activated at the muscle.

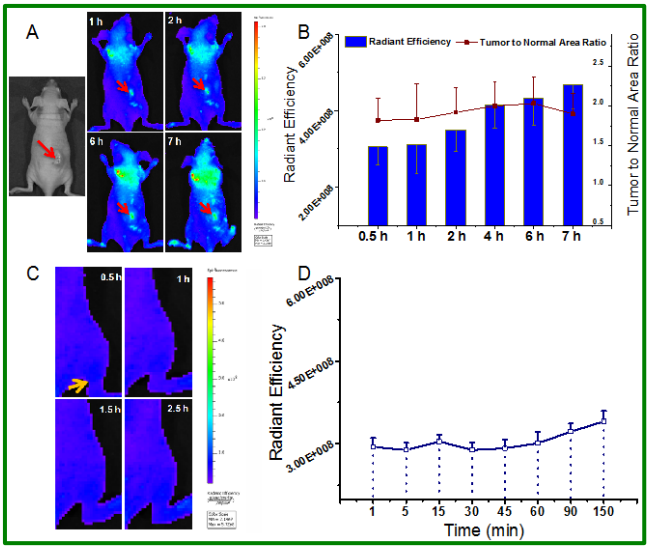

Figure 6. In vivo imaging for MCF-7 tumor model with moderate expression of MMP-2. (A) Fluorescence images at various time points after i.v. injection. (B) The radiant efficiency and tumor to normal area ratio in the tumor site. (C) In vivo imaging following intramuscular injection at various time points. (D) The radiant efficiency in the intramuscular injection site.

Brain tumor imaging

Gliomas account for about 80% of all malignant brain tumors, [20] imposing great health risks globally. MMP-2 is overexpressed in gliomas, and actively involved in rapid cellular proliferation, increased motility, invasion, and angiogenesis of gliomas.[21] Therefore, MMP-2 would be an ideal target for brain tumor detection and imaging. At first, we used the subcutaneous glioma xenograft model for investigating the applicability of the nanoprobe for imaging. The results showed the nanoprobe was preferentially activated in the tumor site within 1 h, and the fluorescence signal gradually intensified (**Figure 7A&B**). At 24 h post-administration, the major organs were collected for imaging. It was found that the tumor tissue displayed the highest fluorescence intensity (**Figure 7C&D**).

This activation pattern was well in accordance with the MMP-2 expression, which was high in the both subcutaneous and orthotopic U87 xenografts, but absent in the normal brain tissue (**Figure 7E**). Moreover, the MMP-2 level was low in the cultured U87 cells but greatly upregulated in the transplanted U87 xenografts. It suggested that the tumor cells could be remodeled by the communication with their surroundings.

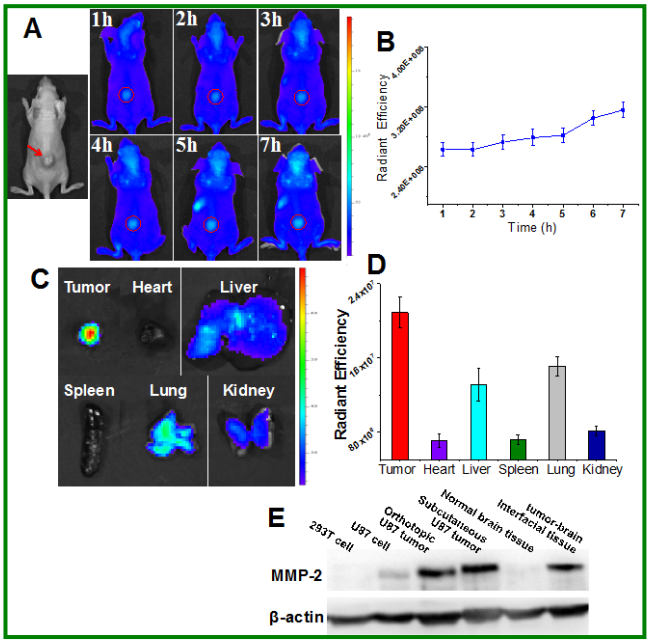

Figure 7. In vivo imaging for U87 glioma model with overexpression of MMP-2. (A) Fluorescence images at various time points after i.v. injection. (B) The radiant efficiency in the tumor site. (C) Ex vivo tissue imaging at the experimental endpoint. (D) Radiant efficiency in the collected tissues. (E) The western blotting assay of MMP-2 expression in tumors and the cultured cells.

However, the in vivo detection of brain tumor is severely impeded by poor penetration through the BBB of the probes. The subcutaneous glioma xenograft model is not sufficient to reflect the clinical conditions. We thus employed the orthotopic glioma mouse model. The development of orthotopic glioma xenograft (U87-Luc cell line) was confirmed by giving luciferin substrate (**Figure 8A**, left panel). The brain-targeting T7 sequence was incorporated into the ALMWP so as to improve the accumulation of the nanoprobe in the brain tumor. The T7-functionalized nanoprobe was administered via tail vein injection. The nanoprobe was activated in the brain tumor quickly (within 1 h). The orthotopic brain tumor was clearly detected, indicating the ability to penetrate through the BBB and target to the glioma cells, as well as the efficient activation by the overexpressed MMP-2 at tumor. The fluorescence gradually increased in 10 h, and was found a declination at 22 h. By contrast, the nanoprobe without T7 modification showed very minor effect presumably due to its insufficient efficiency of brain delivery (data not shown). Furthermore, the orthotopic xenograft was processed with cryosection, the activated nanoprobes were found in the tumor (Supplementary Material: **Figure S5**).

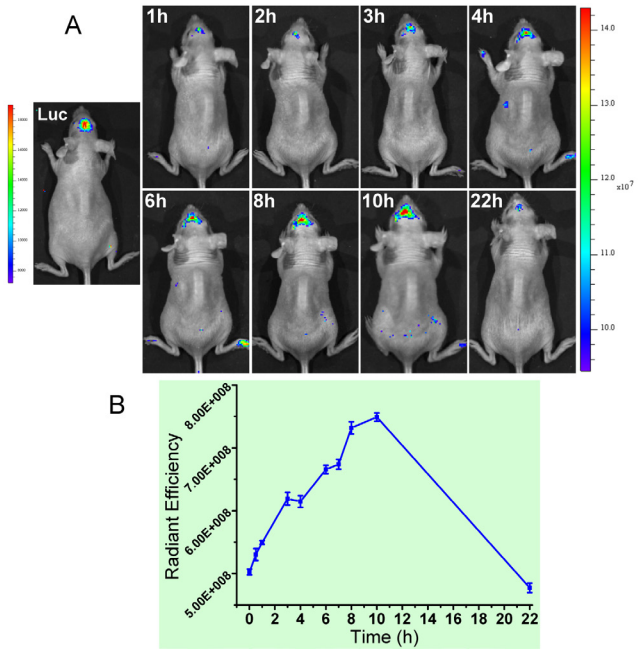

Figure 8. (A) The orthotopic glioma imaging with the T7-functionalized nanoprobe at various time points. (B) The radiant efficiency (fluorescence intensity).

Preliminary toxicity assessment of the nanoprobes

The biocompatibility of the nanoprobe was investigated in non-tumoral 293T and HUVEC cell lines. The results showed that LMWH modification remarkably improved the biocompatibility of QD; the prepared nanoprobes exhibited a dose-dependent inhibitory effect on cell growth, and cell viability at 250 μg/mL was all above 70% (**Figure 9A&B**). Of note, the dose for in vivo imaging was far much less than that.

The in vivo assessment was further performed on KM mice. Dosage used in the each injection was 10 mg/kg, and the animals were given two injections in 2 weeks. The nanoprobe had no significant effect on body weight compared to the blank group (**Figure 9C**). At the endpoint, the organ coefficients showed no significant changes in the heart, liver, lung and kidney between the QD-LMWH group and nanoprobe group, compared with the blank group (**Figure 9D**). However, the spleen coefficients in both QD-LMWH group and nanoprobe group showed significantly increase compared with the blank group, especially in the QD-LMWH group, which may due to the accumulation in the spleen.

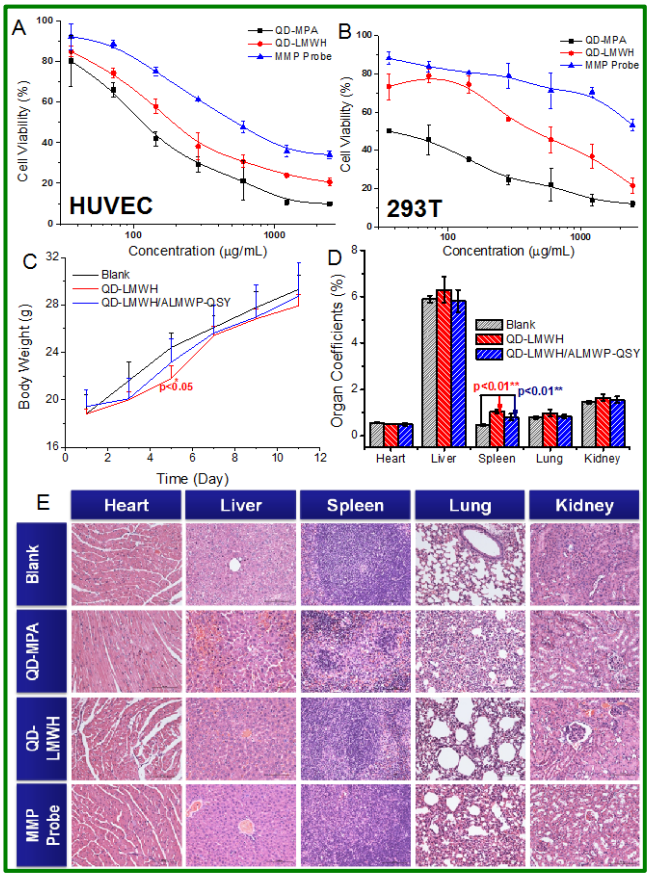

Figure 9. Preliminary safety evaluation of the nanoprobe. Cell viability studies in HUVEC cells (A) and 293T cells (B). (C) The change of the body weight over the regimen. (D) The organ coefficients after treatment. (E) Histological examination of heart, liver, spleen, lung, and kidney. The nanoprobe caused little changes in the organs, while the QD-MPA induced severe toxicity.

Furthermore, the organs were processed by histopathological examination. Results showed that the QD-MPA treated animals developed severe lesions in the heart, liver, spleen, lung and kidney. QD-LMWH treated animals had slight lesions. By contrast, histological examination from the nanoprobe group and saline group displayed no distinguishable changes, suggesting the promise of reduced side effects.

Conclusion

Tumor-associated proteases are the important regulators in cancer development. MMP-2 is involved in carcinogenesis, featured by overexpression in tumor tissues. The MMP-2-activatable nanoprobe was developed for in vivo tumor detection and imaging. This self-assembling nanoprobe remained quenched due to the FRET effect, and could be efficiently activated in the tumors with high level of MMP-2, thereby achieving tumor targeting. The functionality of tumor detection and imaging was demonstrated in various animal tumor models (e.g. fibrosarcoma and glioma cancer). Brain tumor detection and imaging still remain a formidable challenge due to the imper-

meable the BBB. By incorporation of the brain-targeting T7 peptide, the nanoprobe was able to penetrate into the orthotopic brain tumor xenograft, and the subsequent activation rendered a clear detection of the tumor, with high contrast to other normal tissues. Therefore, the protease-activatable nanoprobe provides a potential method for tumor imaging, and moreover, the tumor-preferential activation offers a useful tool for real-time detection of a tumor-associated protease. In particular, it would be potential for brain tumor detection and imaging.

Supplementary Material

Fig.S1 – S5. http://www.thno.org/v05p0787s1.pdf

Acknowledgements

We thank the support from National Basic Research Program of China (973 Program 2013CB932503, 2014CB931900) and NSFC of China (91029743, 81172996, 81373357, 81361140344, 81422048).

Competing Interests

The authors have declared that no competing interest exists.

References

1. Mason SD, Joyce JA. Proteolytic networks in cancer. Trends Cell Biol. 2011; 21: 228-37.
2. Egeblad M, Werb Z. New functions for the matrix metalloproteinases in cancer progression. Nat Rev Cancer. 2002; 2: 161-74.
3. Brinckerhoff CE, Matrisian LM. Matrix metalloproteinases: a tail of a frog that became a prince. Nat Rev Mol Cell Biol. 2002; 3: 207-14.
4. Roy R, Yang J, Moses MA. Matrix metalloproteinases as novel biomarkers and potential therapeutic targets in human cancer. J Clin Oncol. 2009; 27: 5287-97.
5. Temma T, Hanaoka H, Yonezawa A, et al. Investigation of a MMP-2 Activity-Dependent Anchoring Probe for Nuclear Imaging of Cancer. PLoS One. 2014; 9: e102180.
6. Chang CH, Huang YL, Shyu MK, et al. Sphingosine-1-phosphate induces VEGF-C expression through a MMP-2/FGF-1/FGFR-1-dependent pathway in endothelial cells in vitro. Acta Pharmacol Sin. 2013; 34: 360-6.
7. Kanayama H, Yokota K, Kurokawa Y, et al. Prognostic values of matrix metalloproteinase-2 and tissue inhibitor of metalloproteinase-2 expression in bladder cancer. Cancer. 1998; 82: 1359-66.
8. Koutroulis I, Zarros A, Theocharis S. The role of matrix metalloproteinases in the pathophysiology and progression of human nervous system malignancies: a chance for the development of targeted therapeutic approaches? Expert Opin Ther Targets. 2008; 12: 1577-86.
9. Jiang T, Olson ES, Nguyen QT, et al. Tumor imaging by means of proteolytic activation of cell-penetrating peptides. Proc Natl Acad Sci U S A. 2004; 101: 17867-72.
10. Wang Y, Jiang Y, Zhang M, et al. Protease-Activatable Hybrid Nanoprobe for Tumor Imaging. Advanced Functional Materials. 2014; 24: 5443-53.
11. Huang Y, Park YS, Moon C, et al. Synthetic skin-permeable proteins enabling needleless immunization. Angew Chem Int Ed Engl. 2010; 49: 2724-7.
12. Wang H, Zhao Y, Wang H, et al. Low-molecular-weight protamine-modified PLGA nanoparticles for overcoming drug-resistant breast cancer. J Control Release. 2014; 192C: 47-56.
13. Yang YX, Jiang YF, Wang Z, et al. Skin-permeable quaternary nanoparticles with layer-by-layer structure enabling improved gene delivery. Journal of Materials Chemistry. 2012; 22: 10029-34.
14. Kuang Y, An S, Guo Y, et al. T7 peptide-functionalized nanoparticles utilizing RNA interference for glioma dual targeting. Int J Pharm. 2013; 454: 11-20.
15. Shen X, Fang J, Lv X, et al. Heparin impairs angiogenesis through inhibition of microRNA-10b. J Biol Chem. 2011; 286: 26616-27.
16. Ma L, Qiao H, He C, et al. Modulating the interaction of CXCR4 and CXCL12 by low-molecular-weight heparin inhibits hepatic metastasis of colon cancer. Invest New Drugs. 2012; 30: 508-17.
17. Kabelac M, Zimandl F, Fessl T, et al. A comparative study of the binding of QSY 21 and Rhodamine 6G fluorescence probes to DNA: structure and dynamics. Phys Chem Chem Phys. 2010; 12: 9677-84.
18. Sariahmetoglu M, Crawford BD, Leon H, et al. Regulation of matrix metalloproteinase-2 (MMP-2) activity by phosphorylation. FASEB J. 2007; 21: 2486-95.
19. Van Wart HE, Birkedal-Hansen H. The cysteine switch: a principle of regulation of metalloproteinase activity with potential applicability to the entire matrix metalloproteinase gene family. Proc Natl Acad Sci U S A. 1990; 87: 5578-82.
20. Goodenberger ML, Jenkins RB. Genetics of adult glioma. Cancer Genet. 2012; 205: 613-21.
21. Badiga AV, Chetty C, Kesanakurti D, et al. MMP-2 siRNA inhibits radiation-enhanced invasiveness in glioma cells. PLoS One. 2011; 6: e20614.